Macromolecules **2002,** *35,* 2365−2374

Modes of Crystallization in Block Copolymer Microdomains: Breakout, Templated, and Confined

Yueh-Lin Loo[†,§] **and Richard A. Register***[,†,‡]

Department of Chemical Engineering and Princeton Materials Institute, Princeton University, Princeton, New Jersey 08544-5263

Anthony J. Ryan

The Polymer Centre, Department of Chemistry, University of Sheffield, Sheffield S3 7HF, United Kingdom

Received October 19, 2001; Revised Manuscript Received January 3, 2002

ABSTRACT: We examined the melt and solid-state structures of a series of diblock copolymers containing polyethylene as the minority block, with a rubbery hydrocarbon majority block. When the interblock segregation strength during crystallization is sufficiently high (approximately 3 times the segregation strength at the order−disorder transition), crystallization can be effectively confined within spherical domains formed by microphase separation in the melt; the process is homogeneously nucleated, and the resulting kinetics are first-order (Avrami $n = 1$). Below this critical interblock segregation strength, crystallization disrupts the spherical microdomains, resulting in sigmoidal kinetics ($n > 1$). Cylinder-forming materials are more complex: there exists a range of intermediate segregation strength where crystallization is templated but not wholly confined within the nanoscale domains prescribed by microphase separation; while the melt morphology is generally retained on cooling, local distortions and connections between cylinders occur due to crystallization. These intercylinder connections allow the material initially contained within several cylinders to be crystallized by a single nucleus, producing sigmoidal kinetics and a dramatic acceleration of the overall crystallization rate, despite the general preservation of the cylindrical structure.

Introduction

Semicrystalline block copolymers can exhibit considerable morphological richness, arising from the two forces which can drive structure development:[1−8] microphase separation between unlike blocks in the melt, which favors the formation of nanometer length scale domains (e.g., spheres, cylinders, lamellae), and crystallization of one block, which favors the formation of alternating amorphous and crystalline layers. When the noncrystallizing block is glassy during crystallization, the overall melt structure is retained: crystallization occurs within the nanoscale domains prescribed by microphase separation,[3,9−17] leading to a “structure-within-structure” morphology. But when the amorphous matrix is nonglassy during crystallization, these two driving forces compete, and the overall structure can differ considerably from that established by self-assembly in the melt. Early reports on weakly segregated polymers containing polyethylene blocks demonstrated the dominance of crystallization in the solid-state structure development process: the melt mesophase was destroyed upon crystallization and an alternating lamellar superstructure established, frequently with a spherulitic superstructure.[4,6,18] However, we recently studied a polyethylene-*b*-poly(styrene-*r*-ethylene-*r*-butene) diblock copolymer (E/SEB) whose matrix is above its glass transition during crystallization and found that crystallization can indeed be confined to the E spheres established in the melt, provided the interblock segregation strength is sufficiently strong.[19] Confining crystallization to within block copolymer microdomains impacts its kinetics drastically:[19,20] crystallization is initiated homogeneously (a rarity in bulk polymers), and the observed crystallization kinetics are first-order rather than the sigmoidal (Avrami-type) kinetics conventionally observed during polymer crystallization.

Crystallization within cylindrical microdomains surrounded by rubbery matrices was also studied by Quiram et al.,[18,21] in polyethylene-*b*-poly(3-methyl-1-butene) diblocks. While small-angle X-ray scattering (SAXS) indicated the preservation of the hexagonal lattice of cylinders when the segregation strength was sufficiently high,[18] these materials nonetheless exhibited conventional sigmoidal crystallization kinetics which did not differ markedly from those observed in less-segregated diblocks where crystallization entirely “rewrites” the structure present in the melt.[21] This contrasts starkly with the glassy-matrix case,[20] where confinement within cylinders leads to first-order crystallization kinetics, exactly as for spheres.

Motivated by this apparent discrepancy, and by our findings of fully confined crystallization in the E/SEB diblock, we set out to explore the degree to which fluid matrices are effective in confining crystallization in block copolymers, for both spherical and cylindrical microdomain geometries. We probe the solid-state morphology by both SAXS and transmission electron microscopy (TEM) and employ time-resolved X-ray scattering to study crystallization kinetics; our previous findings on crystallization in glassy-matrix diblocks[20] show that the crystallization kinetics are highly sensitive to the connectivity of the crystallizable material,

---

* To whom correspondence should be addressed: e-mail register@princeton.edu.

[†] Department of Chemical Engineering.

[‡] Princeton Materials Institute.

[§] Present address: Bell Laboratories, Lucent Technologies, 600 Mountain Ave., Murray Hill, NJ 07974.

10.1021/ma011824j CCC: $22.00

Table 1. Characteristics of Semicrystalline Diblocks with Rubbery Matrices

sample	total M_n (kg/mol)	w_E[a]	$w_{1,2}$ B block	E $T_{m,peak}$[b] (°C)	E $T_{c,peak}$[b] (°C)	w_c[c]	T_{ODT}[d] (°C)	melt structure
E/SEB 5/30	35.1	0.14	0.085	103	57	0.34	200	E spheres
E/SEB 6/39	45.0	0.14	0.073	100	60	0.36	263	E spheres
E/SEB 9/55	63.7	0.14	0.082	101	62	0.37	>300	E spheres
E/SEB 10/63	73.8	0.14	0.068	101	63	0.35	>300	E spheres
E/SEB 17/52	69.8	0.25	0.071	105	63	0.32	>300	E cylinders
E41	41	1	0.083	105	84	0.33		

[a] Target w_E. [b] Measured by DSC at 10 °C/min. [c] Fractional crystallinity of E block; heat of fusion from DSC trace normalized by w_E and $\Delta H_m^0 = 277$ J/g.[25] [d] Order−disorder transition temperature, measured via SAXS on heating.

even connections through infrequent defect structures which are difficult to detect in the ensemble-average scattering pattern.

Experimental Section

Synthesis and Molecular Characterization. The precursors to the E/SEB diblocks, poly(high-1,4-butadiene)-*b*-poly(styrene-*r*-butadiene), were synthesized via sequential anionic polymerization at 60 °C in cyclohexane under vacuum. The butadiene block was polymerized first, initiated by *tert*-butyllithium. After polymerization of the first block was complete, an aliquot was withdrawn for characterization, and then tetramethylethylenediamine (TMEDA) was added at a 4:1 TMEDA:Li molar ratio along with the appropriate charge of styrene and butadiene (70/30 weight ratio for all diblocks). In addition to randomizing the styrene−butadiene monomer sequence,[22] as verified by ozonolysis,[23] TMEDA also enhances the 1,2-enchainment of butadiene, to approximately 46%. Gel permeation chromatography (GPC) showed the diblocks to have a polydispersity < 1.2 and to be free from detectable terminated first block (<0.2 wt %). The precursors were then selectively hydrogenated, as described previously,[24] over a Ni/Al catalyst that saturates olefinic (>99%) but not aromatic units. Molecular characteristics of the E/SEB diblocks, and a hydrogenated high-1,4 polybutadiene homopolymer prepared similarly (E41), are given in Table 1. The molecular weight of the first (B) block was determined by GPC, and the diblock molecular weight was calculated from this value in combination with the known monomer charges. Because both blocks contain butadiene, ^{1}H NMR cannot be used to determine a diblock composition unambiguously. However, the ratios of butadiene to styrene resonances were in all cases consistent with the targeted block composition (hereafter expressed as w_E, the weight fraction of E block in the E/SEB diblock) and styrene:butadiene ratio in the second block (70:30 w/w), indicating that the true value of w_E does not differ substantially from the target.

The synthesis and characterization of the E/MB diblocks have been described previously.[18] Briefly, precursor poly(high-1,4-butadiene)-*b*-poly(high-3,4-isoprene) diblocks were synthesized anionically, using 1,2-dipiperidinoethane as the modifier for the second (polyisoprene) block. These precursors were exhaustively saturated to produce the E/MB diblocks, where “MB” denotes 3-methyl-1-butene, the predominant monomer residue in the saturated diblock (which is in fact a statistical terpolymer of 3-methyl-1-butene, 2-methyl-1-butene, and ethylene−propylene units).[9]

All diblocks employed in this work are denoted by the block chemistry (E/SEB or E/MB) and a two-number suffix (e.g., 9/55) which indicates the approximate number-average molecular weights M_n of the two blocks, in kg/mol.

Differential Scanning Calorimetry. The peak melting temperature, $T_{m,peak}$, and heat of melting, ΔH_m, of each diblock were obtained on heating at 10 °C/min using a Perkin-Elmer DSC-7 equipped with an Intracooler II and calibrated with indium and tin. Specimens were first crystallized on cooling at 10 °C/min from the melt to establish a common thermal history. The E block fractional crystallinity, w_c, was then calculated from ΔH_m:

$$w_c = \frac{\Delta H_m}{w_E \Delta H_m^0} \tag{1}$$

where w_E is the E block weight fraction (see Table 1), and ΔH_m^0 is the heat of fusion of 100% crystalline polyethylene (taken as 277 J/g).[25] The onset crystallization temperature, $T_{c,onset}$, of the E block of each diblock sample was obtained on cooling at 10 °C/min. The glass transition temperature (T_g, midpoint) of SEB in all four of the E/SEB diblock copolymers was located at 25 ± 2 °C on heating at 10 °C/min. The constancy of T_g across this series of diblocks confirms that the precursor to the SEB block has the same composition (70 wt % styrene targeted) in all cases.

Transmission Electron Microscopy. Prior to staining and sectioning, different thermal histories were imposed on the sphere-forming E/SEB diblocks using the Perkin-Elmer DSC-7: either quenching from the melt to room temperature at a nominal cooling rate of 50 °C/min or quenching to a predetermined crystallization temperature and holding isothermally for several times the crystallization half-time. The cylinder-forming samples were flow-aligned in the melt at 150 °C in a lubricated channel die[26] and allowed to crystallize on cooling at approximately 10 °C/min before staining. Slivers of the diblocks were stained by immersion in 0.5 wt % RuO_4 stabilized aqueous solution (Electron Microscopy Sciences): 12 h for E/SEB diblocks and 14 h for E/MB 17/45. After staining, the slivers were embedded in LR White medium-grade acrylic resin (Structure Probe), sectioned at room temperature to ca. 60 nm using a diamond knife, collected on copper grids covered with holey carbon, and examined at 100 keV on a Zeiss 910 TEM. Because of the low T_g of MB (−17 °C),[18] the E/MB 17/45 samples were placed in a −15 °C freezer for 2 h prior to sectioning.

Static Small-Angle X-ray Scattering (SAXS). Static SAXS profiles were collected using an Anton-Paar compact Kratky camera equipped with a position-sensitive detector (Braun OED-50M). The data were reduced using previously reported procedures[27] to obtain profiles of desmeared intensity vs scattering vector, q, where $q = (4\pi/\lambda) \sin \theta$; λ is the radiation wavelength (Cu Kα) and 2θ is the scattering angle. We were able to determine, or place lower bounds upon, the order−disorder transition temperature (T_{ODT}, see Table 1) by monitoring the SAXS profiles as a function of temperature.[28]

Time-Resolved Small and Wide-Angle X-ray Scattering (SAXS/WAXS). Time-resolved simultaneous SAXS/WAXS experiments were conducted on beamline 8.2 at the Daresbury Laboratory, U.K., using an incident beam of $\lambda = 0.154$ nm and a Linkam DSC 600 for temperature control.[4,6,29] Sample preparation, data acquisition, and data reduction procedures, including a time adjustment to compensate for temperature gradients during temperature scanning, have been described in detail elsewhere.[19,20,23] Isothermal crystallizations were conducted by heating the specimen into the melt ($T_m < T < T_{ODT}$), quenching at approximately 40 °C/min to a predetermined crystallization temperature, and holding isothermally while the structural changes due to crystallization were monitored through time-resolved SAXS/WAXS. The WAXS data showed the same time course as the SAXS data,[19] but with a poorer signal-to-noise ratio because of the modest fraction of crystallizable block, so only SAXS data are presented here.

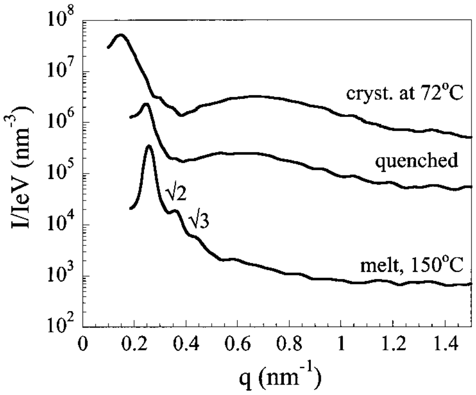

Figure 1. SAXS profiles acquired on E/SEB 5/30 in the melt at 150 °C (bottom profile), at room temperature after quenching from the melt into liquid nitrogen (middle profile), and at 72 °C after being held isothermally for 180 min (top profile).

Results and Discussion

1. Sphere-Forming Diblocks. We studied four E/SEB diblocks, all of which form E spheres in the melt, to explore how interblock segregation strength affects crystallization. The diblocks have identical compositions (w_E); segregation strength was varied through diblock molecular weight (see Table 1). Previously, we reported[19] that the E blocks in E/SEB 9/55 crystallized within the spheres established by microphase separation in the melt, for all crystallization conditions employed. The higher molecular weight E/SEB 10/63 behaves similarly, so here we focus on the two lower molecular weight E/SEB diblocks, E/SEB 5/30 and E/SEB 6/39, where crystallization is *not* always confined within spheres. Both of these diblocks have accessible ODT temperatures (Table 1). Taking the mean-field prediction[30] that the ODT occurs at a fixed value of χN_t for a given block copolymer composition, where χ is the Flory segmental interaction parameter between the two blocks and N_t is the total degree of polymerization of the diblock, we can use these two T_{ODT} values to estimate[31] that at 60 °C (typical for E block crystallization in these materials) E/SEB 5/30 and E/SEB 6/39 have $(\chi N_t)/(\chi N_t)_{ODT}$ values of approximately 1.8 and 2.3, while E/SEB 9/55 has a ratio of approximately 3.2.

Morphology. Figure 1 displays static SAXS profiles for E/SEB 5/30. The bottom profile, acquired in the melt at 150 °C, reveals a sharp primary peak and higher-order reflections at q/q^* ratios of $\sqrt{2}$ and $\sqrt{3}$, indicating that the E spheres are arranged on a body-centered-cubic (bcc) lattice in the melt.[32] The middle SAXS profile, acquired after the specimen had been quenched from the melt into liquid nitrogen and allowed to warm to room temperature, retains a narrow primary peak at essentially the same position q^*, indicating that the melt structure of E/SEB 5/30 is largely retained on quenching.[19] The broad hump observed in the vicinity of $q = 0.6$ nm^{-1} results from the crystallites within the E spheres. The top SAXS profile in Figure 1 was acquired after isothermal crystallization at 72 °C for 180 min (crystallization half-time $t_{1/2} \approx 20$ min at 72 °C) and is significantly different from the other two SAXS profiles. The primary peak has shifted to lower q and broadened significantly, indicating that the melt lattice has been destroyed upon crystallization. Thus, the solid-state structure of E/SEB 5/30 depends strongly on thermal history: quenching traps the melt structure while a slower crystallization, such as that conducted isothermally at 72 °C, permits major structural rearrangement. A similar thermal history dependence was found in the SAXS profiles for E/SEB 6/39 (not shown).

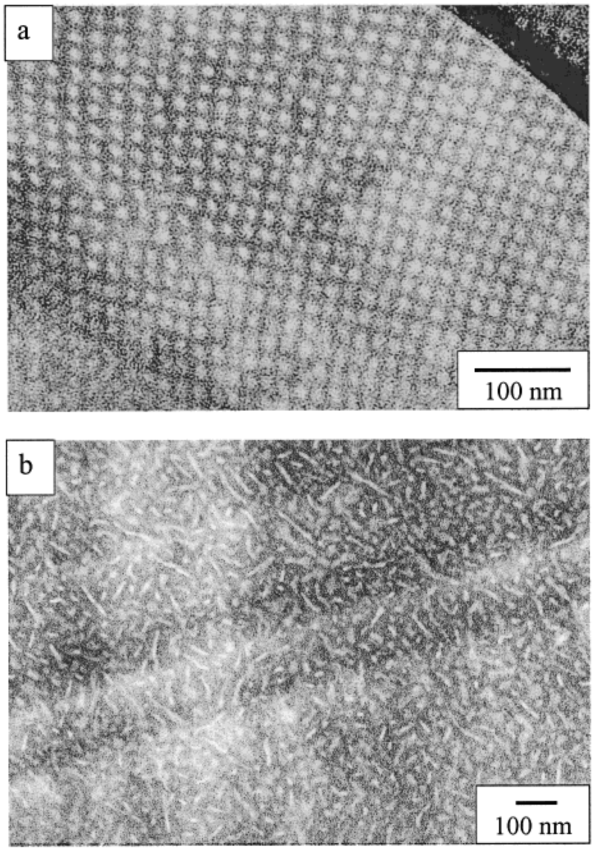

Figure 2. TEM images of fully crystallized E/SEB 5/30 after undergoing different crystallization histories: (a) quenched from the melt to room temperature at 50 °C/min; (b) isothermally crystallized at 64 °C for 20 min. SEB matrix is stained dark with RuO_4.

TEM images of E/SEB 5/30 following both quenching and isothermal crystallization, shown in Figure 2, confirm the inferences drawn from the SAXS data. RuO_4 reacts preferentially with styrene residues,[33] staining the SEB matrix dark. Under the staining conditions employed, both amorphous and crystalline E appear light and cannot be distinguished from each other. The quenched specimen (Figure 2a) shows spherical microdomains on a regular lattice, while the specimen crystallized isothermally at 64 °C (Figure 2b) shows very little resemblance to the bcc melt structure: the E domains (light in the image) are elongated into rods or disks, and the lattice has been completely destroyed. Analogous micrographs for E/SEB 6/39 are shown in Figure 3, again showing preservation of the bcc lattice in the quenched specimen and substantial distortion of the lattice during isothermal crystallization ($t_{1/2} < 1$ min at 64 °C for both diblocks). Side-by-side comparison of Figures 2b and 3b reveals less “breakout” in the more strongly segregated E/SEB 6/39: what appear to be remnants of the original spheres and even of the regular lattice are evident, and none of the E microdomains show the elongated character evident for E/SEB 5/30 in Figure 2b. This suggests that the higher segregation strength in E/SEB 6/39 more strongly opposes structural rearrangement during crystallization.

While the mechanism underlying the “breakout” is not directly revealed in Figures 2b and 3b, we consider two

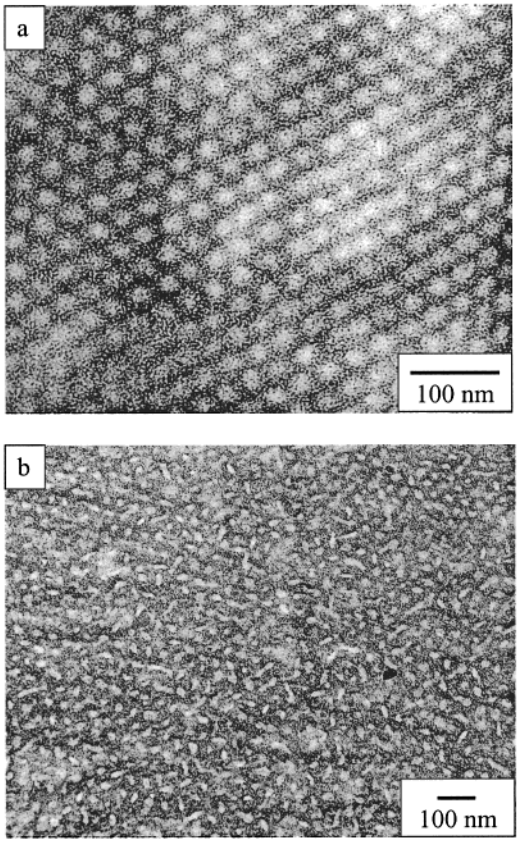

Figure 3. TEM images of fully crystallized E/SEB 6/39 after undergoing different crystallization histories: (a) quenched from the melt to room temperature at 50 °C/min; (b) isothermally crystallized at 64 °C for 20 min. SEB matrix is stained dark with RuO_4.

possibilities. The first is distortion of the microdomain interface by the growing crystal; sufficient distortion could allow the interfaces of neighboring microdomains to meet, permitting extended crystal growth. The second mechanism would simply involve the diffusion of block copolymer chains between microdomains, which would allow chains to add to the growing crystal in one microdomain at the expense of others. For lengths comparable to the distance between microdomains (order 20 nm here), chain diffusion is still relatively facile even in strongly segregated polymers.[34]

The ability to preserve the bcc lattice in fast-cooled specimens of E/SEB 5/30 and E/SEB 6/39 begs the question: would more strongly segregated materials, such as E/SEB 9/55, show "breakout" if crystallization were sufficiently slow? This question is difficult to answer with absolute certainty, but we have found that E/SEB 9/55 shows confined crystallization even under excruciatingly slow crystallization conditions. Figure 4 shows a TEM image of E/SEB 9/55 taken after isothermal crystallization at 70 °C for 3.5 h, where the crystallization half-time $t_{1/2}$ is approximately 60 min. The regular lattice of E spheres is still clearly evident. This should be compared with the TEM images of E/SEB 5/30 (Figure 2b) and E/SEB 6/39 (Figure 3b) taken after relatively fast isothermal crystallization ($t_{1/2} < 1$ min). SAXS patterns[23] acquired on E/SEB 9/55 crystallized under similarly slow conditions (>70 °C, not presented here) also show retention of the primary peak position. Therefore, while we cannot *prove* that confined crystallization is the state of lowest free energy in E/SEB 9/55 and 10/63, it is at least a robustly metastable state, as it forms under every crystallization condition we have employed.

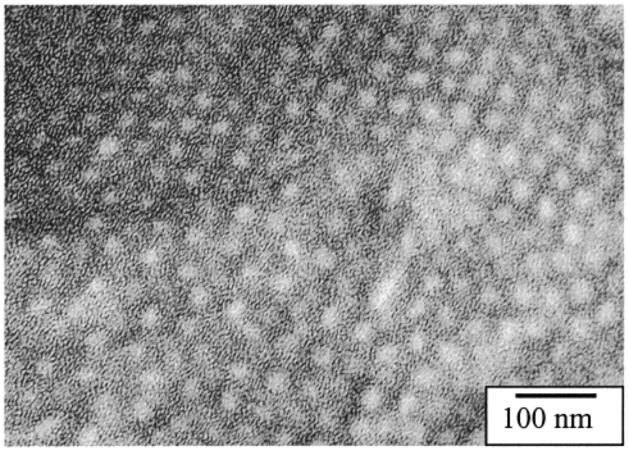

Figure 4. TEM images of fully crystallized E/SEB 9/55 after isothermal crystallization at 70 °C for 3.5 h. SEB matrix is stained dark with RuO_4.

On the other hand, we note that it is certainly plausible that confined crystallization *is* the equilibrium structure in these materials, in part because the E block (hydrogenated polybutadiene) is effectively a random copolymer of ethylene and butene, with the butene weight fraction ($w_{1,2}$) given in Table 1. At room temperature, hydrogenated polybutadienes of this microstructure possess average crystal thicknesses of approximately 5 nm and crystallinities of 30−35 wt %.[6,35] Thus, the crystals need not experience any reduction in thickness upon confinement, since the spheres in E/SEB 9/55 have diameters of 25 nm. Moreover, the weight fraction crystallinity of the E blocks in E/SEB 9/55 and 10/63 determined by DSC (see Table 1) are essentially the same as in the hydrogenated polybutadiene homopolymer E41, presumably because the large amorphous fraction allows the modest fractional crystallinity to be easily accommodated in a microdomain with curved surfaces. Indeed, in E/SEB 9/55, a disklike crystal 5 nm thick in the center of the sphere (25 nm diam) would occupy precisely 30% of the sphere volume. In the remainder of this discussion, we consider a material to exhibit confined crystallization behavior if it does so under every crystallization condition examined, including slow isothermal crystallizations ($t_{1/2} >$ 5 min).

Kinetics. "Breakout" and crystal confinement are substantially different in their crystallization kinetics as well. Previously,[19] we showed that confined crystallization in E/SEB 9/55 resulted in first-order kinetics, where crystallization was initiated by homogeneous nucleation within each individual spherical microdomain (25 nm diameter). Since E crystal growth across the entire sphere is essentially instantaneous once nucleated, the overall crystallization kinetics simply reflect the rate at which the E microdomains nucleate. However, the situation is radically altered when the crystals are no longer confined to the microdomains in which they were nucleated. Figure 5 contains a series of SAXS profiles collected during isothermal crystallization of E/SEB 5/30 at 67 °C. As crystallization proceeds, the higher-order reflections associated with the bcc lattice gradually disappear, while the primary peak shifts to lower q and broadens significantly. To quantify this process, we monitored the SAXS intensity integrated over the region of the primary peak in the

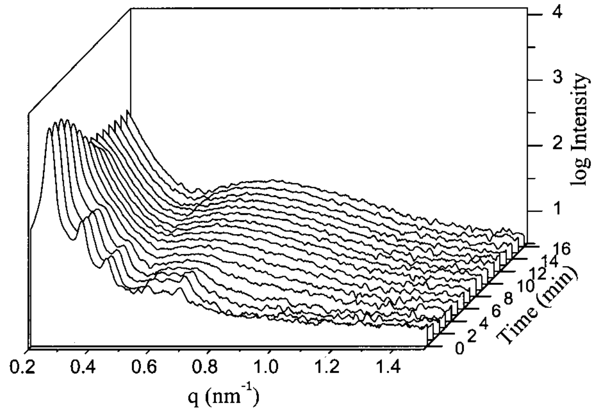

Figure 5. SAXS profiles taken during isothermal crystallization of E/SEB 5/30 at 67 °C; the specimen reaches 67 °C at time = 0. Each profile is accumulated over 1 min beginning at the time indicated. The higher resolution of the synchrotron beamline permits additional reflections ($\sqrt{5}$, $\sqrt{6}$, $\sqrt{7}$) from the bcc melt structure to be observed beyond those in Figure 1.

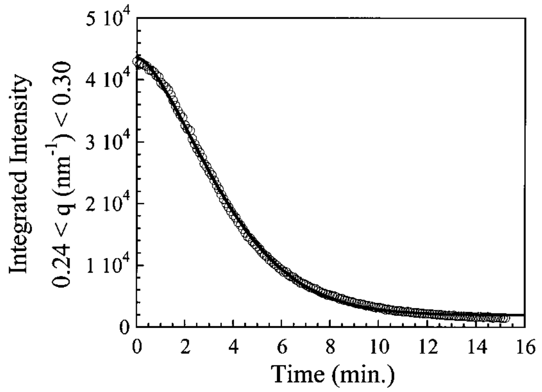

Figure 6. Time course of the integrated SAXS intensity at the position of the melt primary peak ($0.24 < q < 0.30$ nm^{-1}) during isothermal crystallization of E/SEB 5/30 at 67 °C. The solid line is the best fit of the Avrami equation to the data, yielding $n = 1.6$ and $t_{1/2} = 3.5$ min.

melt (total intensity over $0.24 < q < 0.30$ nm^{-1}, no baseline subtraction), as plotted in Figure 6. The data are well-described by the Avrami equation:[19,20,36,37]

$$1 - y = \exp(-kt^n) \qquad (2)$$

where y represents the fraction of the crystallization process that has occurred at time t, k is the rate constant, and n is the Avrami exponent. Fitting the data in Figure 6 to eq 2 yields $n = 1.6$ and a corresponding crystallization half-time $t_{1/2} = 3.5$ min. These sigmoidal crystallization kinetics are not qualitatively different from those of homopolymers (though n is smaller than usual[37]) and directly reflect the structural rearrangement which occurs upon crystallization. Since a nucleus generated in one sphere can ultimately crystallize the E blocks from several spheres, crystal growth (to its final extent) does *not* occur much faster than nucleation, as it does in E/SEB 9/55. Rather, as time progresses, the crystals originating from one nucleus in E/SEB 5/30 span a progressively greater volume of material until the supply of E begins to be exhausted, much as in spherulitic crystallization of homopolymers. The isothermal crystallization kinetics for E/SEB 6/39 (not shown) were also sigmoidal, qualitatively similar to those for E/SEB 5/30.

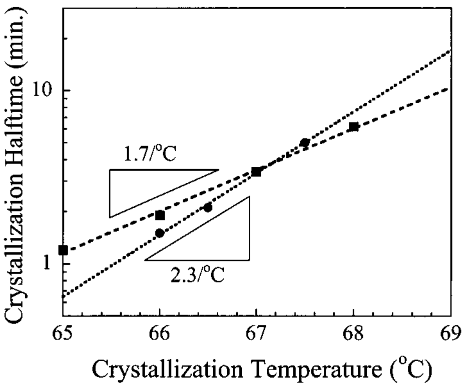

Figure 7. Crystallization half-times, $t_{1/2}$, for E/SEB 5/30 (■) and E/SEB 6/39 (●). Both materials exhibit sigmoidal crystallization kinetics. Lines represent the best exponential fits to the data, with the temperature dependences indicated.

Crystallization halftimes $t_{1/2}$ for E/SEB 5/30 and E/SEB 6/39 are compiled in Figure 7. For E/SEB 6/39, $t_{1/2}$ increases with crystallization temperature by a factor of 2.3/°C, while for E/SEB 5/30, $t_{1/2}$ increases by a factor of 1.7/°C. A statistical t-test indicates that these values differ at better than the 99.9% confidence level. These may be compared with temperature dependences which we have reported previously[19] for related materials: 2.9/°C in E/SEB 9/55, where crystallization is confined within spheres and the temperature dependence reflects the rate of nucleation; 1.4/°C for the hydrogenated polybutadiene homopolymer E41, which exhibits spherulitic crystallization and where the temperature dependence of the crystallization rate largely reflects the temperature dependence of the rate of crystal growth. The deep undercoolings required to crystallize E/SEB 5/30 and E/SEB 6/39 (see Figure 7), comparable to those in E/SEB 9/55, suggest that crystallization proceeds via homogeneous nucleation in E/SEB 5/30 and 6/39 as well. The homogeneous nucleation rate for pure E at any temperature, $\dot{N}(T)$, was previously established[19,23] from measurements on E/SEB 9/55. Therefore, the number of homogeneous nuclei generated during isothermal crystallization of E/SEB 5/30 and E/SEB 6/39, N, can be estimated as[20,23]

$$N \approx v_E \dot{N}(T) t_{1/2} \qquad (3)$$

where v_E is the volume fraction of E block (spheres, here). With $\dot{N}(T) = 7 \times 10^{16}$ nuclei/cm^{3}min for E at 66 °C,[19] eq 3 yields an estimated density of 2×10^{16} homogeneous nuclei/cm^3 generated upon isothermal crystallization at 66 °C in both E/SEB 5/30 and 6/39. For comparison, the number densities of microdomains in these materials are 8×10^{16} and 4×10^{16} per cm^3, respectively, suggesting that each nucleus crystallizes the E blocks which initially formed a few spheres. These calculated values of N far exceed the typical density of active impurities within hydrogenated polybutadiene homopolymers ($\approx 10^9$ nuclei/cm^3),[35] indicating that crystallization in these two diblocks is still homogeneously nucleated.[19]

Though the analysis above demonstrates that E/SEB 5/30, 6/39, and 9/55 are all homogeneously nucleated, they still show substantially different temperature dependences for the overall crystallization rate (see Figure 7). To elucidate the origin of this difference, we conducted isothermal crystallization of E/SEB 5/30 at higher temperatures; while impractically slow to con-

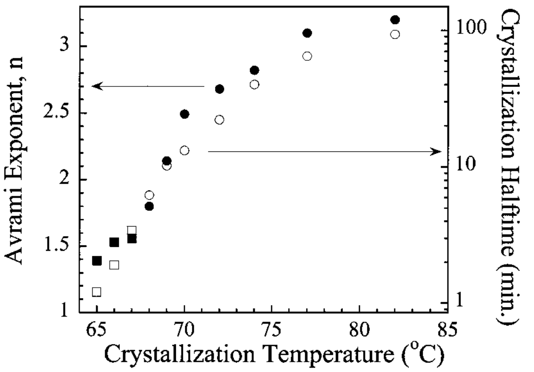

Figure 8. Right axis, open symbols (□, ○): crystallization half-time, $t_{1/2}$, for E/SEB 5/30 during isothermal crystallization. Left axis, filled symbols (■, ●): Avrami exponent, *n*, extracted from fit of same isothermal crystallization data to eq 2. Squares represent data acquired at Daresbury; circles represent data acquired on the laboratory-based Kratky camera.

duct at the synchrotron, these were easily executed on the same laboratory-based setup used to generate the static SAXS patterns. Figure 8 shows that as the crystallization temperature increases, the temperature dependence of the crystallization rate becomes smaller, and the Avrami exponent *n* increases. These two effects have a common origin: as the crystallization temperature is increased, the rate of homogeneous nucleation is decreased, allowing each nucleus time to crystallize the E material from a larger number of spherical microdomains before the supply of E is exhausted. This causes the half-time locus to curve systematically downward from a simple extrapolation of the low-temperature data with a slope of 2.9/°C (the slope found for E/SEB 9/55). As for the Avrami exponent, Figures 1 and 2a show that confined crystallization can be achieved in E/SEB 5/30 when crystallization is rapid; thus, $n = 1$ is expected for E/SEB 5/30 at low temperatures, where each nucleus crystallizes only a single sphere. By contrast, at high temperatures, *n* should approach the value[37] of 4 expected for a constant nucleation rate and three-dimensional growth,[38] as each nucleus crystallizes the E material from a large number of spheres. The largest value of *n* which we actually measure is 3.2, close to this limit. This progressive change in the amount of material crystallized by each nucleus also explains the unexpected crossing of the half-time loci for E/SEB 5/30 and 6/39 in Figure 7. In the low-temperature limit, where crystallization is confined within spheres, E/SEB 6/39 crystallizes more rapidly because the individual spheres are larger than in E/SEB 5/30 (and only one nucleus is required to crystallize an entire sphere, regardless of size). At higher temperatures, however, the extent of “breakout” is greater in E/SEB 5/30 (compare Figures 2b and 3b), meaning that the effective rate of crystal growth is faster and hence the half-time shorter for E/SEB 5/30.

2. Cylinder-Forming Diblocks. Confined Crystallization. Our previous studies of E crystallization within glassy block copolymer mesophases (in polyethylene−poly(vinylcyclohexane) diblocks[20]) demonstrated that the connectivity of the crystallizable material strongly impacts the crystallization kinetics and that diblocks containing either spheres or cylinders of E (discrete microdomains) both exhibit first-order kinetics initiated by homogeneous nucleation. Here, we explore the analogous case where the matrix is above its T_g during crystallization and ask whether strict confinement can still be achieved (and if so, under what conditions). Figure 9 shows SAXS patterns for E/SEB 17/52, a cylinder-forming diblock of the same block chemistry as the sphere-formers discussed in the previous section. The melt profile shows a narrow primary peak at $q^* = 0.121$ nm^{-1}, followed by a series of higher-order peaks at q/q^* ratios of $\sqrt{3}$, $\sqrt{4}$, and $\sqrt{7}$, characteristic of a hexagonally packed array of long cylinders.[32] E/SEB 17/52 remains ordered up to at least 300 °C and thus may be considered strongly segregated during E block crystallization. The top SAXS profile in Figure 9 was acquired at room temperature after E/SEB 17/52 had been fully crystallized on cooling at approximately 8 °C/min; judging from the narrow primary peak, at essentially the same q^* as in the melt, crystallization is effectively confined within the cylinders. The TEM images in Figure 10 confirm this inference: here, the specimen was flow-aligned prior to crystallization, and the two images were taken on cross sections cut perpendicular (Figure 10a) and parallel (Figure 10b) to the flow direction (cylinder axis). We observe cylinders end-on and side-on, respectively, indicating that the melt microdomains are retained on crystallization, though the long-range order of the microdomains is relatively poor; this reduced long-range order is also evident in the solid-state SAXS profile in Figure 9, where the higher-order reflections are absent. Previous work[9] has shown that when polyethylene is confined within block copolymer cylinders, the *b*-axis (fast growth direction) of the polyethylene crystals is generally aligned with the cylinder axis. The reduced long-range order presumably results from local distortions induced by the crystals as they grow along the cylinders.

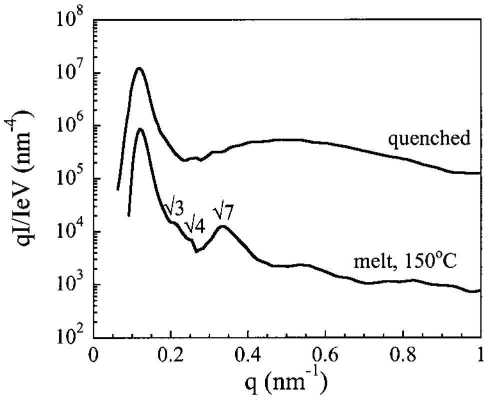

Figure 9. One-dimensional SAXS profiles of E/SEB 17/52 taken in the melt at 150 °C (bottom profile) and at room temperature after the sample had been fully crystallized on cooling at 8 °C/min (top profile). The higher-order reflections associated with the hexagonal lattice are highlighted in the melt profile.

The isothermal crystallization kinetics of E/SEB 17/52 were also examined. Figure 11 represents the time evolution of the intensity of the SAXS crystallite “hump” (integrated over $0.23 < q < 0.82$ nm^{-1}) during isothermal crystallization at 69.5 °C. The crystallization process is well described by a first-order fit, as expected for complete confinement of the growing crystals within individual cylinders. These results indicate that sufficiently strong interblock segregation can effectively restrict crystallization to within the individual block copolymer cylinders despite a rubbery matrix.

Templated Crystallization. Previously, Quiram et al.[18,21] reported on the crystallization behavior of cylinder-forming E/MB diblocks covering a range of molecular

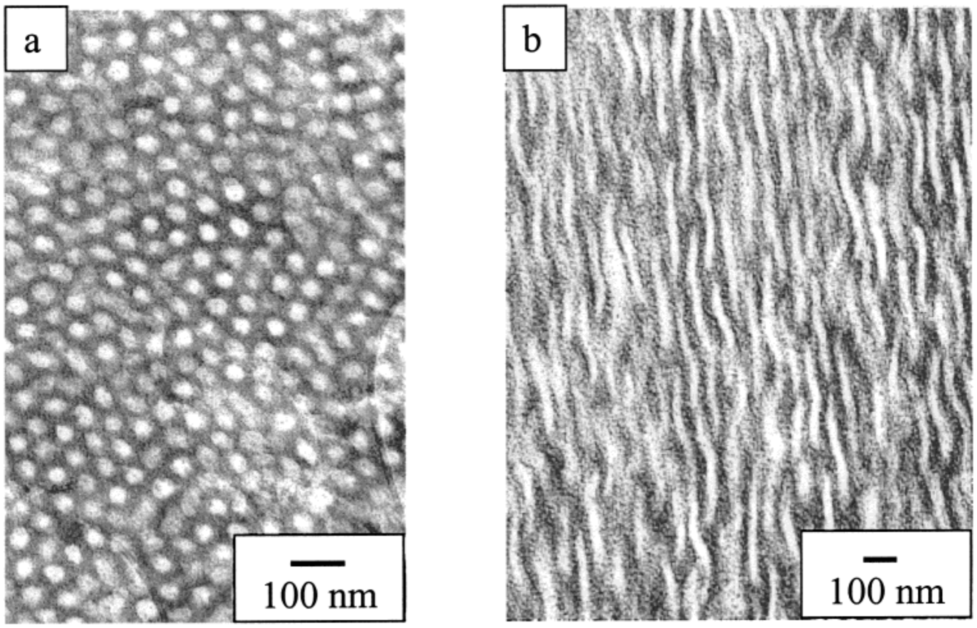

Figure 10. TEM images of fully crystallized E/SEB 17/52, oriented by channel die compression and crystallized on cooling at 10 °C/min: (a) cross section perpendicular to the cylinder axis; (b) cross section parallel to the cylinder axis. SEB matrix is stained dark with RuO_4.

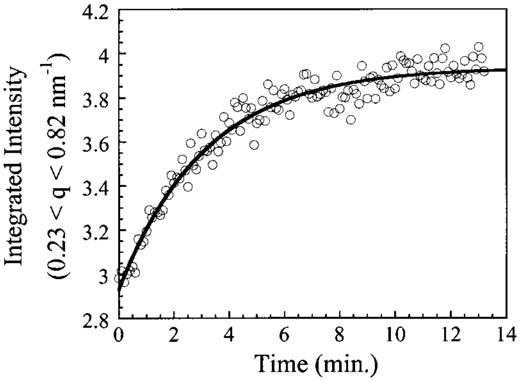

Figure 11. Time course of the integrated SAXS intensity in the region of the crystallite "hump" ($0.23 < q < 0.82$ nm^{-1}) during isothermal crystallization of E/SEB 17/52 at 69.5 °C. Solid line represents first-order fit to data, yielding a crystallization half-time of 2.2 min.

weights at fixed composition, analogous to the E/SEB series used here to study crystallization within spheres. For the most strongly segregated E/MB diblocks, static SAXS measurements indicated that crystallization was confined: one-dimensional SAXS patterns showed retention of the primary peak position, while two-dimensional SAXS on flow-aligned specimens showed retention of the hexagonal packing of cylinders.[18] However, these same specimens also showed sigmoidal crystallization kinetics as measured by either time-resolved SAXS/WAXS[21] or DSC.[39] Indeed, the crystallization kinetics of these strongly segregated E/MB diblocks more closely resembled those of E/MB diblocks of lower molecular weight, even one which crystallized from a homogeneous melt, rather than the cylinder-forming E/SEB described above.

Here, we identify the origin of this apparent discrepancy through TEM, with Figure 12 showing images taken on flow-aligned E/MB 17/45. Since the E/MB diblocks are entirely composed of saturated hydrocarbon, staining contrast arises purely from the difference in RuO_4 uptake in the different phases.[33] MB and amorphous E are both above their T_g at room temperature and stain at similar rates, so we were unable to resolve the outlines of the block copolymer microdomains. However, the E crystals stain far more slowly, so white E crystallites can be discerned upon a background of stained amorphous E and MB. Figure 12a represents a cross section perpendicular to the cylinder axis while Figure 12b represents a cross section parallel to the cylinder axis. In Figure 12b, the E crystals are clearly evident, generally running diagonally in the image; however, several crystallites can be observed (example highlighted in the white oval) running transverse to this general orientation. Similar "rogue" crystals can be seen in Figure 12a, connecting what would ideally be a hexagonal array of white spots.

These "rogue" crystals running between cylinders produce the observed sigmoidal crystallization kinetics, since extended crystal growth (spanning several cylinders) can occur from a single nucleus through these connections. This is also reflected in the temperature dependence of the overall crystallization rate of E/MB 17/45, as shown in Figure 13, where $t_{1/2}$ increases by only a factor of 1.2/°C with crystallization temperature, similar to the value of 1.4/°C measured for the hydrogenated polybutadiene homopolymer E41. By contrast, E/SEB 17/52 exhibits a slope of 2.5/°C, comparable to the value of 2.9/°C for the sphere-forming E/SEB 9/55[19] and to the value of 2.2/°C found for E crystallization in cylinders confined by a glassy VCH matrix,[20] all of which show first-order kinetics. Comparison of the half-times shown for E/SEB 17/52 and E/MB 17/45 in Figure 13 makes clear the dramatic acceleration of the overall crystallization rate produced by these intercylinder connections.

At 76 °C, the homogeneous nucleation density calculated according to eq 3 is 5×10^9 nuclei/cm^3 for E/MB 17/45, comparable to the typical density of heterogeneous nuclei. Thus, we cannot definitively establish the nucleation mechanism in this material. However, the key point is that regardless of how crystallization is initiated, occasional "rogue" crystals can allow large

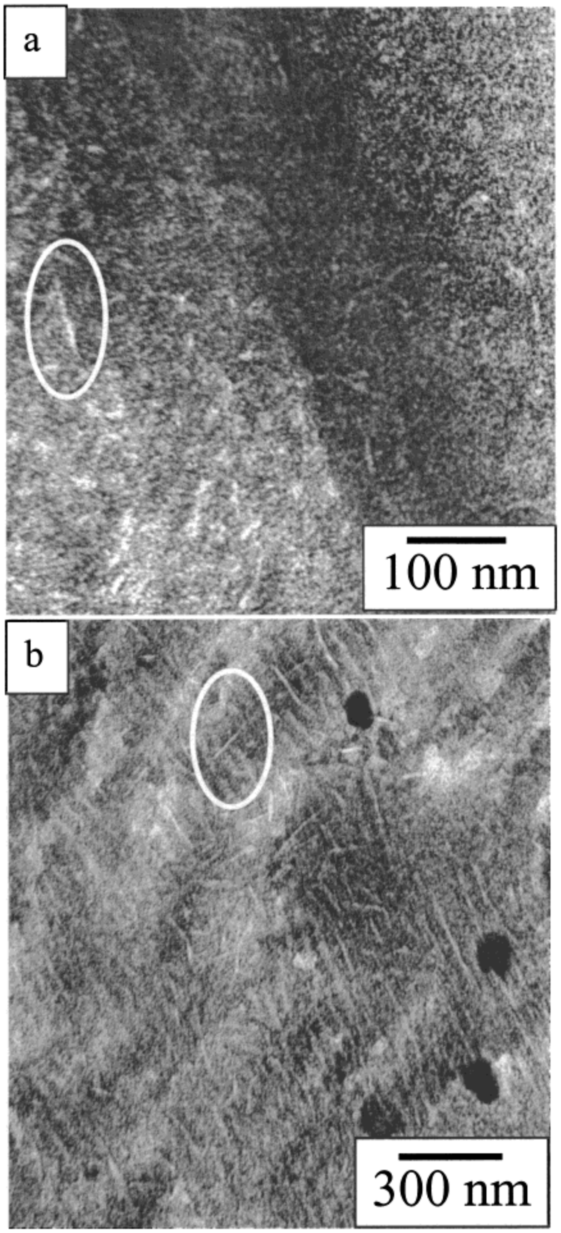

Figure 12. TEM images of fully crystallized E/MB 17/45, oriented by channel die compression and crystallized on cooling at 10 °C/min: (a) cross section perpendicular to the cylinder axis; (b) cross section parallel to the cylinder axis. Amorphous E and MB are both stained dark with RuO_4. White ovals highlight "rogue" crystals which run between microdomains.

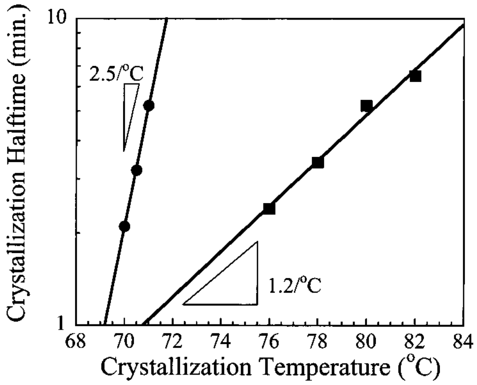

Figure 13. Crystallization half-times, $t_{1/2}$, for cylinder-forming semicrystalline diblocks: E/MB 17/45 (■), which exhibits sigmoidal crystallization kinetics, and E/SEB 17/52 (●), which exhibits first-order crystallization kinetics. Lines represent the best exponential fits to the data, with the temperature dependences indicated.

volumes of material to be crystallized by a single nucleus, while still allowing the cylinders present in the melt to template the orientation of the great majority of the crystallized E.

3. Classification Map. Thus, these rubbery-matrix semicrystalline block copolymers show three general types of crystallization: confined (static SAXS indicates melt morphology largely retained, first-order crystallization kinetics); unconfined (homogeneous melt) or "breakout" (static SAXS indicates melt morphology destroyed, sigmoidal crystallization kinetics); and templated (static SAXS indicates melt morphology largely retained, sigmoidal crystallization kinetics). The results presented in the preceding sections suggest that which of these three types is manifested depends on both the segregation strength and on melt morphology (spheres vs cylinders). If these two factors dominate, then it should be possible to present the results in the form of a classification map with segregation strength and morphology as the two axes. For morphology, we simply choose as the relevant variable the volume fraction of E block, v_E. For segregation strength, χN_t could be used; however, $(\chi N_t)_{ODT}$ is a also a strong function of composition (v_E), so we normalize by this factor and consider the ratio $(\chi N_t)_c/(\chi N_t)_{ODT}$, where the subscript c indicates that χN_t is evaluated at the crystallization temperature (peak T_c on cooling, listed in Table 1 for E/SEB and in ref 21 for E/MB diblocks).

The interaction parameter $\chi_{E/SEB}(T)$ can be estimated from the T_{ODT} values for E/SEB 5/30 and 6/39; counting each styrene or butadiene mer in the precursor polymer in the calculation of N_t and taking[30] $(\chi N_t)_{ODT} = 27$ at $v_E = 0.17$:

$$\chi_{E/SEB}(T) = -0.052 + \frac{52.9}{T\ (K)} \tag{4}$$

Similarly, for $\chi_{E/MB}(T)$, based on T_{ODT} for E/MB 11/32 and bounds on T_{ODT} for E/MB 8/24 and 17/45,[18,39] with[30] $(\chi N)_{ODT} = 16$ at $v_E = 0.28$, we obtain

$$\chi_{E/MB}(T) = -0.003 + \frac{12}{T\ (K)} \tag{5}$$

From these expressions, we calculate that $(\chi N_t)_c/(\chi N_t)_{ODT}$ is approximately 5.2 for E/SEB 17/52 and 1.9 for E/MB 17/45. Values of $(\chi N_t)_c/(\chi N_t)_{ODT}$ estimated in this manner are given in Table 2 for all diblocks studied here, as well as the remaining E/MB diblocks studied previously by Quiram et al.[21,39]

Figure 14 shows a map classifying the regions where the three types of crystallization are found. For sphere formers, only confined and "breakout" crystallization are observed, with the boundary between them occurring at approximately $(\chi N_t)_c/(\chi N_t)_{ODT} \approx 3$. For cylinders, an intermediate region of "templated" crystallization occurs, with the boundary between templated and "breakout" occurring at about $(\chi N_t)_c/(\chi N_t)_{ODT} \approx 1.5$. Thus, even moderately segregated cylinders can effectively guide crystallization. At very high values of $(\chi N_t)_c/(\chi N_t)_{ODT}$, crystallization can be confined within cylinders even when the matrix is rubbery; our limited data do not allow us to firmly determine the dividing line between templated and confined crystallization in cyl-

Table 2. Interblock Segregation Strengths for Semicrystalline Diblocks with Rubbery Matrices

sample	spheres or cylinders of E	sphere or cylinder radius[a] (nm) at 150 °C	$(\chi N)_{ODT}$[b]	$((\chi N)_c)/((\chi N)_{ODT})$	crystallization behavior
E/SEB 5/30	S	9.4	27	1.8	breakout
E/SEB 6/39	S	10.7	27	2.3	breakout
E/SEB 9/55	S	13.6	27	3.2	confined
E/SEB10/63	S	15.3	27	3.7	confined
E/SEB 17/52	C	17.0	19	5.2	confined
E/MB 8/24	C	*c*	16	0.96	unconfined[c]
E/MB 11/32	C	9.0	16	1.3	breakout
E/MB 17/45	C	12.8	16	1.9	templated
E/MB 23/63	C	14.5	16	2.7	templated

[a] Determined from SAXS primary peak position, using the known v_E and the symmetry of the bcc lattice. [b] Estimated from ref 30 at the known v_E. [c] E/MB 8/24 crystallizes from a homogeneous melt ($T_c > T_{ODT}$); the primary SAXS peak in the solid state is substantially shifted from the correlation hole peak in the melt (see ref 18).

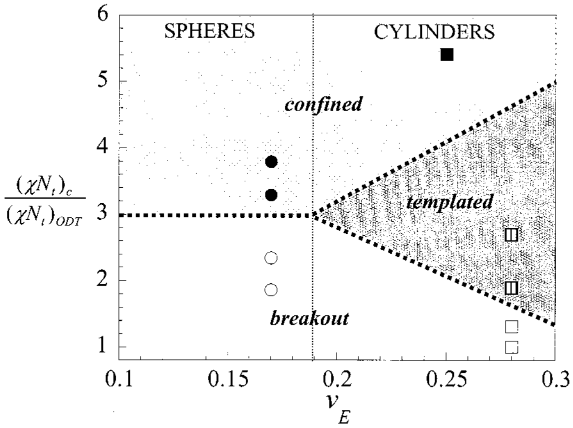

Figure 14. Classification map of crystallization modes in semicrystalline diblocks with rubbery matrices. Open symbols represent samples where the melt mesophase was completely destroyed on cooling (breakout) or where the melt was homogeneous (unconfined); symbols with vertical hatch represent templated crystallization; and filled symbols represent confined crystallization. Circles represent diblocks forming spheres of E; squares represent cylinders. The bold dashed lines are guides to the eye, approximately dividing the region of breakout (bottom) from the region of confinement (top, light hatch) and the region of templated crystallization (right center, heavy hatch).

inders, but Figure 14 suggests that it occurs at approximately $(\chi N_t)_c/(\chi N_t)_{ODT} \approx 4 \pm 1$.

Templated crystallization is observed in cylinder-forming samples and not sphere-forming samples because in the former, the occasional "rogue" crystals connecting cylinders do not impact the overall structure significantly, since the cylinders are long (order 1 μm). Two such connection events per cylinder, while sufficient to permit crystals to percolate throughout the entire specimen, would have little effect on the average structure probed by SAXS. By contrast, the isometric microdomains in sphere-forming samples would no longer be spheres if each were connected to the positions of two neighboring microdomains.

In the construction of Figure 14, we have assumed that only the morphology (v_E) and normalized segregation strength $(\chi N_t)_c/(\chi N_t)_{ODT}$ are relevant parameters. In fact, the polymers represented in Figure 14 differ in molecular weight, glass transition temperature, and entanglement molecular weight, to name a few other material parameters. Though it is possible that each of these factors may have some independent influence on the crystallization behavior, the general success of Figure 14 at classifying the mode of crystallization suggests that segregation strength and morphology are indeed the two most important parameters.

Conclusions

Through a combination of static SAXS, TEM, and crystallization kinetics measurements, we have delineated three modes of crystallization in diblock copolymers forming spheres or cylinders of E in a rubbery matrix: breakout, templated crystallization, and confined crystallization. These classifications correspond to the behavior observed during slow crystallizations; the most strongly segregated specimens exhibited confined crystallization under all conditions, even when crystallization required hours to complete. For spheres, the boundary between breakout and confined crystallization occurs when the normalized segregation strength, $(\chi N_t)_c/(\chi N_t)_{ODT}$, is approximately 3. For cylinders, there is an intermediate region of templated crystallization, extending over roughly $1.5 < (\chi N_t)_c/(\chi N_t)_{ODT} < 4$, where the cylinders formed by microphase separation in the melt generally guide the growing crystals but do not wholly confine them. Occasional "rogue" crystals connecting different cylinders, observed directly by TEM, allow a large volume of material to be crystallized from a single nucleus, producing conventional sigmoidal crystallization kinetics and an overall crystallization rate dramatically faster than for confined crystallization. Nonetheless, since these "rogue" crystals are infrequent, the static SAXS patterns from samples exhibiting templated crystallization are indistinguishable from those where crystallization is truly confined to the cylinders in which the nuclei originated. These observations reveal the limitations of static SAXS in assessing whether crystallization is truly confined: only in the case of spheres does a percolating network of crystals (two connections per microdomain) necessarily eradicate the lattice present in the melt. For other morphologies, even cylinders, probes which are more sensitive to infrequent defects (such as TEM) are needed to establish the degree of crystal confinement. Time-resolved SAXS is particularly useful in this regard, as it provides both an ensemble-average structural measurement and information on the crystallization kinetics, which are highly sensitive to the degree of connectivity of the crystallizable material.

Acknowledgment. Financial support for this study came from the National Science Foundation, Polymers Program (DMR-9711436). The authors also thank EPSRC for Daresbury beamtime under Grant GR/M22116 to A.J.R. Y.-L.L. acknowledges the Princeton University Graduate School for the Porter Ogden Jacobus Fellowship.

References and Notes

(1) Hamley, I. W. *Adv. Polym. Sci.* **1999**, *148*, 113.

(2) Chen, H.-L.; Hsiao, S.-C.; Yamauchi, K.; Hasegawa, H.; Hashimoto, T. *Macromolecules* **2001**, *34*, 671.

(3) Zhu, L.; Cheng, S. Z. D.; Calhoun, B. H.; Ge, Q.; Quirk, R. P.; Thomas, E. L.; Hsiao, B. S.; Yeh, F.-J.; Lotz, B. *J. Am. Chem. Soc.* **2000**, *122*, 5957.

(4) Rangarajan, P.; Register, R. A.; Adamson, D. H.; Fetters, L. J.; Bras, W.; Naylor, S.; Ryan, A. J. *Macromolecules* **1995**, *28*, 1422.

(5) Mai, S.-M.; Fairclough, J. P. A.; Viras, K.; Gorry, P. A.; Hamley, I. W.; Ryan, A. J.; Booth, C. *Macromolecules* **1997**, *30*, 8392.

(6) Ryan, A. J.; Hamley, I. W.; Bras, W.; Bates, F. S. *Macromolecules* **1995**, *28*, 3860.

(7) Nojima, S.; Kato, K.; Yamamoto, S.; Ashida, T. *Macromolecules* **1992**, *25*, 2237.

(8) Hong, S.; Yang, L. Z.; Macknight, W. J.; Gido, S. P. *Macromolecules* **2001**, *34*, 7009.

(9) Quiram, D. J.; Register, R. A.; Marchand, G. R.; Adamson, D. H. *Macromolecules* **1998**, *31*, 4891.

(10) Weimann, P. A.; Hajduk, D. A.; Chu, C.; Chaffin, K. A.; Brodil, J. C.; Bates, F. S. *J. Polym. Sci., Part B: Polym. Phys.* **1999**, *37*, 2053.

(11) Loo, Y.-L.; Register, R. A.; Adamson, D. H. *Macromolecules* **2000**, *33*, 8361.

(12) Loo, Y.-L.; Register, R. A.; Adamson, D. H. *J. Polym. Sci., Part B: Polym. Phys.* **2000**, *38*, 2564.

(13) Lotz, B.; Kovacs, A. J. *Polym. Prepr. (Am. Chem. Soc., Div. Polym. Chem.)* **1969**, *10* (*2*), 820.

(14) Zhu, L.; Cheng, S. Z. D.; Calhoun, B. H.; Ge, Q.; Quirk, R. P.; Thomas, E. L.; Hsiao, B. S.; Yeh, F.-J.; Lotz, B. *Polymer* **2001**, *42*, 5829.

(15) Cohen, R. E.; Cheng, P. L.; Douzinas, K.; Kofinas, P.; Berney, C. V. *Macromolecules* **1990**, *23*, 324.

(16) Hamley, I. W.; Fairclough, J. P. A.; Ryan, A. J.; Bates, F. S.; Towns-Andrews, E. *Polymer* **1996**, *37*, 4425.

(17) Hamley, I. W.; Fairclough, J. P. A.; Terrill, N. J.; Ryan, A. J.; Lipic, P. M.; Bates, F. S.; Towns-Andrews, E. *Macromolecules* **1996**, *29*, 8835.

(18) Quiram, D. J.; Register, R. A.; Marchand, G. R. *Macromolecules* **1997**, *30*, 4551.

(19) Loo, Y.-L.; Register, R. A.; Ryan, A. J. *Phys. Rev. Lett.* **2000**, *84*, 4120.

(20) Loo, Y.-L.; Register, R. A.; Ryan, A. J.; Dee, G. T. *Macromolecules* **2001**, *34*, 8968.

(21) Quiram, D. J.; Register, R. A.; Marchand, G. R.; Ryan, A. J. *Macromolecules* **1997**, *30*, 8338.

(22) Chang, C. C.; Halasa, A. F.; Miller, J. W., Jr.; Hsu, W. L. *Polym. Int.* **1994**, *33*, 151.

(23) Loo, Y.-L. Ph.D. Thesis, Princeton University, 2001.

(24) Adams, J. L.; Quiram, D. J.; Graessley, W. W.; Register, R. A.; Marchand, G. R. *Macromolecules* **1998**, *31*, 201.

(25) Brandrup, J., Immergut, E. H., Eds. *Polymer Handbook*, 3rd ed.; Wiley: New York, 1989.

(26) Lee, H. H.; Register, R. A.; Hajduk, D. A.; Gruner, S. M. *Polym. Eng. Sci.* **1996**, *25*, 6137.

(27) Register, R. A.; Bell, T. R. *J. Polym. Sci., Part B: Polym. Phys.* **1992**, *30*, 569.

(28) Adams, J. L.; Quiram, D. J.; Graessley, W. W.; Register, R. A.; Marchand, G. R. *Macromolecules* **1996**, *29*, 2929.

(29) Bras, W.; Derbyshire, G. E.; Devine, A.; Clark, S. M.; Cooke, J.; Komanschek, B. E.; Ryan, A. J. *J. Appl. Crystallogr.* **1995**, *28*, 26.

(30) Matsen, M. W.; Bates, F. S. *Macromolecules* **1996**, *29*, 1091.

(31) Bates, F. S.; Schultz, M. F.; Rosedale, J. H.; Almdal, K. *Macromolecules* **1992**, *25*, 5547.

(32) Sakurai, S.; Hashimoto, T.; Fetters, L. J. *Macromolecules* **1993**, *26*, 5796.

(33) Trent, J. S. *Macromolecules* **1984**, *17*, 2930.

(34) Yokoyama, H.; Kramer, E. J. *Macromolecules* **2000**, *33*, 954.

(35) Rangarajan, P.; Register, R. A.; Fetters, L. J. *Macromolecules* **1993**, *26*, 4640.

(36) Avrami, M. *J. Chem. Phys.* **1939**, *7*, 1103.

(37) Hay, J. N. *Br. Polym. J.* **1971**, *3*, 74.

(38) A straight-line extrapolation of log$\dot{N}$ vs T, using the $t_{1/2}$ data of ref 19, leads to an estimate of $N = 5 \times 10^{10}$ nuclei/cm^3 for E/SEB 5/30 at 82 °C. Though the extrapolation is long, this value of N still substantially exceeds the typical density of heterogeneous nuclei found in hydrogenated polybutadiene ($\approx 10^9$ nuclei/cm^3), so we infer that homogeneous nucleation dominates even at 82 °C. At still higher temperatures, it is possible that heterogeneous nucleation would dominate; $n = 3$ is expected for instantaneous nucleation followed by three-dimensional growth.

(39) Quiram, D. J. Ph.D. Thesis, Princeton University, 1997.

MA011824J